Behavior and Strength Prediction of Concrete Beams reinforced with GFRP Bars and subjected to High Temperature

Maan Hatam Saeed
Department of Civil Engineering, College of Engineering, University of Baghdad, Iraq
Maan.Hatem2101p@coeng.uobaghdad.edu.iq (corresponding author)

Ali Hussein Ali Al-Ahmed
Department of Civil Engineering, College of Engineering, University of Baghdad, Iraq
dr.ali-alahmed@coeng.uobaghdad.edu.iq

Received: 31 October 2024 | Revised: 21 November 2024 | Accepted: 25 November 2024

 DOI: https://doi.org/10.48084/etasr.9454

ABSTRACT

The behavior and strength prediction of concrete beams reinforced with Glass Fiber-Reinforced Polymer (GFRP) bars at high-temperature conditions are examined in this work. Twelve beams burnt at 500°C and 700°C were reviewed as part of the experimental methods, and were contrasted with four more unburned beams. The parameters chosen in this study consist of the type of main bar material, protection type against fire, concrete cover thickness, and the burning temperature. The experimental results indicate that the stiffness of all samples diminishes with rising burning temperatures. This is attributable to the degradation of concrete during the fire being exposed to, leading to an increase in beam deflection under the same load. The plastering of 1 cm was better than the fire-resistant dye as a form of protection against burning, while All beams experienced flexural failure.

Keywords-ASTM E119; plastering; fire resistant dye; elevated temperature; GFRP bars; burning

I. INTRODUCTION

The use of GFRP composites to strengthen concrete components for infrastructure restoration has gained attention in recent decades. For around 40 years, this trend has been consistently observed. The GFRP reinforcement applications are many, including creating new structures and repairing the current ones [1-6]. Authors in [7] illustrated the effects of subjecting typical concrete to elevated temperatures of 400°C and 700°C. Two scenarios of steel reinforcement burning were conducted alongside the exposure of 12 mm steel reinforcement bars. Some of them were directly exposed to high temperatures, namely 400°C and 700°C, while others were shielded with 15 mm of concrete covering. The experimental findings derived from the bars' fire exposure for one hour at 400°C and 700°C, followed by their progressive cooling, indicated that the residual average percentage of compressive strength of concrete was 85.3% and 41.4%, respectively, whereas the remaining average percent of the modulus of elasticity was 75% and 48%, respectively. After burning and cooling under the same circumstances, the average yielding tensile stress (Ø 12.0 mm) was 96.59% and 86.39% for concrete-covered bars and 93.39% and 81.29% for uncovered bars, respectively. Authors in [8] performed experimental evaluations on the fire resistance of concrete beams reinforced with GFRP rebars. Three beam samples were utilized in the fire exposure experiments, focusing on their load-bearing capacity under fire conditions. One specimen was fortified with conventional steel rebars, whilst the other two were enhanced using GFRP rebars. The impact of the concrete quality on fire resistance was examined. The continuous pressures on the beam samples during the fire exposure testing were 60% of the ultimate loads. The behavior of the beams before failure was observed. The utilization of GFRP rebars led to a notable reduction in fire resistance. Authors in [9] investigated the flexural behavior of Fiber-Reinforced Polymer (FRP)-enhanced beams exposed to elevated temperatures. Twenty-five specimens, comprising both unstrengthened and FRP-strengthened beams, were fabricated. Glass and basalt FRP systems were evaluated with and without protective measures, including a cement grout overlay and two varieties of widely accessible intumescent coatings. Two specimens were used to measure the temperature-time histories at various locations, including FRP laminate surfaces, FRP-concrete contact, interior steel bars, and beam centers. The samples were examined for failure under one-point loading after being exposed to high temperatures. As the temperature increased, the specimens' initial stiffness and final strength decreased. When the elevated temperature was below 700°C, the protection systems seemed to preserve the structural integrity of the glass FRP systems. The Basalt FRP-reinforced beams exhibited a lesser reduction in ultimate strength compared to

glass FRP-reinforced beams. Authors in [10] reported the results of computational tests examining the influence of critical factors on the fire behavior of concrete beams strengthened with FRP bars. The model's validity is confirmed by comparing its numerical predictions with empirical data obtained from the fire test. Parametric studies indicate that the type of rebar, the thickness of concrete cover, and the fire scenario significantly influence the fire response of concrete beams reinforced with FRP rebars. The presence of an axial constraint in the beam has a negligible effect on fire resistance.

Authors in [11] examined the fatigue behavior of concrete beams reinforced with FRP bars following exposure to elevated temperatures. Thirteen concrete beams reinforced with glass- and GFRP/CFRP bars were assessed for static and fatigue loading following exposure to varying levels of elevated temperatures. The effects of high temperatures, holding period, fatigue load intensity, and FRP bar type on beam fatigue were all assessed. The findings indicated that elevated temperature exposure adversely impacted the fatigue life of GFRP-reinforced concrete beams more significantly than that of CFRP-reinforced beams at temperatures below 400°C. The GFRP- and CFRP-reinforced beams lost their load-bearing capacity when the exposure temperature neared 600°C. Authors in [12] studied how increased temperatures affect load resistance in concrete beams reinforced with GFRPs. Three specimens were tested at elevated temperatures, 350°C, 500°C, and 600°C, before being subjected to an one-point load until failure. One specimen was tested at ambient temperature. Heating reinforced concrete beams to 350°C, 500°C, and 600°C resulted in a 4%, 15.5%, and 19% loss in loading capacity. Authors in [13] studied both experimentally and numerically the behavior of GFRP-reinforced concrete beams under increased temperatures. The experimental data demonstrated that the shear failure is the most common failure mode in all examined beams. The numerical model was validated against the experimental test results before analyzing the impact of key factors on the performance and ultimate load of GFRP-RC beams at various high temperatures. Authors in [14] examined the load-bearing capacity of FRP-reinforced concrete subjected to high temperatures. The results were juxtaposed with a concrete specimen with steel reinforcement. Economically produced GFRP and CFRP rebars with sand-coated surfaces were evaluated in concrete beams subjected to four-point bending stresses. The residual flexural strength of reinforced concrete heated to 1000°C was assessed, analyzed, and compared to that of the unheated sections. The research indicated that a concrete beam strengthened with a 10 mm glass rebar attained 31% of its initial load-bearing capacity, while a beam reinforced with a 14 mm glass rebar obtained 45.9%. Authors in [15] investigated the effect of higher temperatures on the load resistance of 20 reinforced concrete beams using GFRP bars. Two samples were analyzed at ambient temperature as control beams, whereas the other 18 were exposed to elevated temperatures of 200°C, 400°C, 600°C, and 800°C for 30, 60, and 90 minutes before the submission of a four-point load test until failure. As the temperature and exposure duration increased, the failure modes changed from compression to balance and tensile failure. After one hour of exposure to temperatures of 200°C, 400°C, 600°C, and 800°C, the residual loading capacity of the heated beams diminished by 13%, 17.39%, 32.6%, and 41.3%, respectively, compared to the control beam.

II. EXPERIMENTAL PROGRAM

The experimental program involves the casting and examination of twelve beams burned at different temperatures and compared with an additional four unburned beams. Besides the burning temperature, the parameters that were chosen in this study consist of the main bar material type, protection type against fire, concrete cover thickness. All beams had the same length, width, height, and stirrups, and were subjected to monotonic load after burning. Fourteen beams had main GFRP bars, while the rest of them had main steel bars. To replicate authentic fire disasters, the beams were subjected to high-temperature flames using a specially designed furnace. The chosen temperatures were 500°C and 700°C. The charred beams were gradually cooled by being exposed to ambient laboratory conditions. The beams were subjected to loading until failure to assess the impact of temperature on residual serviceability and the ultimate capacity of each beam, in comparison to the unburned control beams. Figure 1 exhibits the beams' details. All beams had a total length of 2.4 m, a width of 20 cm, and a height of 30 cm. Regarding the type of reinforcement, fourteen beams had longitudinal reinforcement of 4Ø12 mm GFRP, while the rest of the beams had longitudinal steel reinforcement of 4Ø12 mm. Stirrups of 10 mm steel bars were supplied in all beams at 15 cm intervals. The beams were tested in a basic scheme with a 2.1 m effective span. The tested RC beams were split into two major groups. These groups were divided based on the concrete cover thickness selected, 2.5 cm, and 4 cm, and each group was divided into three subgroups based on the degrees of burning temperature chosen, ambient, 500°C, and 700°C. The ambient group contained 2 beams, one beam with steel bars, and the other beam with GFRP bars, while each of the 500°C, and 700°C groups was divided based on the type of the selected protection, plastering 1 cm, fire-resistant dye, and without any protection. Table I exhibits the details of the tested beams. Figure 2 provides the schematic classifications of the beam comparisons, which have been adopted in this study.

TABLE I. DETAILS OF THE EXAMINED BEAMS

Group	Beam ID	Fire Temp. °C	Protection type	Main bars type
Cover 25 mm	GP25H1	500	Plastering 1 cm	GFRP
	GD25H1	500	Fire resistant dye	GFRP
	GW25H1	500	Without	GFRP
	GP25H2	700	Plastering 1 cm	GFRP
	GD25H2	700	Fire resistant dye	GFRP
	GW25H2	700	Without	GFRP
	G25	Amb.	Without	GFRP
	S25	Amb.	Without	Steel
Cover 40 mm	GP40H1	500	Plastering 1 cm	GFRP
	GD40H1	500	Fire resistant dye	GFRP
	GW40H1	500	Without	GFRP
	GP40H2	700	Plastering 1 cm	GFRP
	GD40H2	700	Fire resistant dye	GFRP
	GW40H2	700	Without	GFRP
	G40	Amb.	Without	GFRP
	S40	Amb.	Without	Steel

Table II shows the tensile properties of the steel reinforcing bars, while Table III illustrates the properties of the used GFRP bars. Figure 3 depicts the fire-resistant dye used in this study.

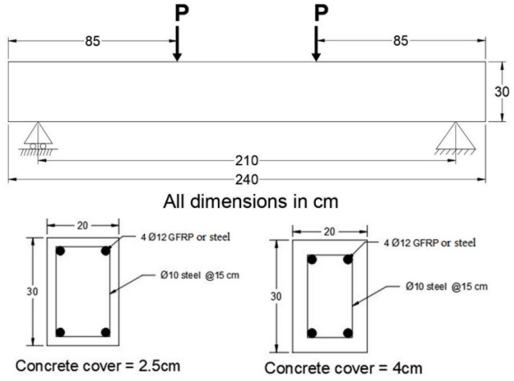

Fig. 1. Details of the tested beams.

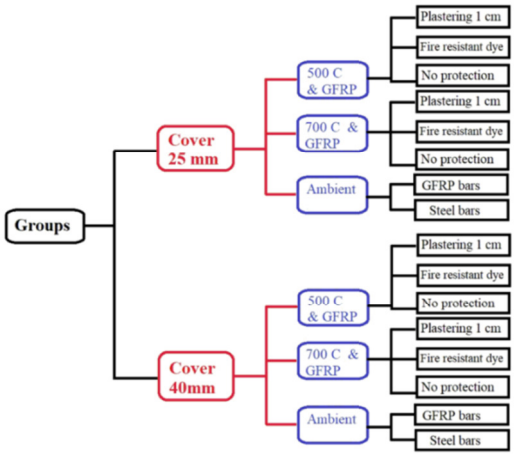

Fig. 2. Group classification for the comparison of the tested beams.

TABLE II. TENSILE PROPERTIES OF THE USED STEEL REINFORCING BARS

Ø (mm)	Yield Tensile Stress, fy (MPa)	Ultimate Tensile Strength, fu (MPa)	Elongation (%)
10	574	660	16.5
12	621	711	14.5

TABLE III. TENSILE PROPERTIES OF THE GFRP BARS

Ø (mm)	Speed (mm/min)	Max. force (N)	Elongation (%)	Tensile strength at break (MPa)
12	6	148147.9	3	1310

Fig. 3. Fire-resistant dye used in this study.

Table IV presents the mix design used to cast the concrete beams. The unburned compressive strength (fc') was 39.66 MPa. Figure 4 displays the wooden molds and steel reinforcement cages of beams.

TABLE IV. MIX PROPORTION

w/c	Mix Proportion (kg/m^3)				
	Cement	Sand	Gravel	Water	Superplasticizer
0.3	470	827	945	147	6.22

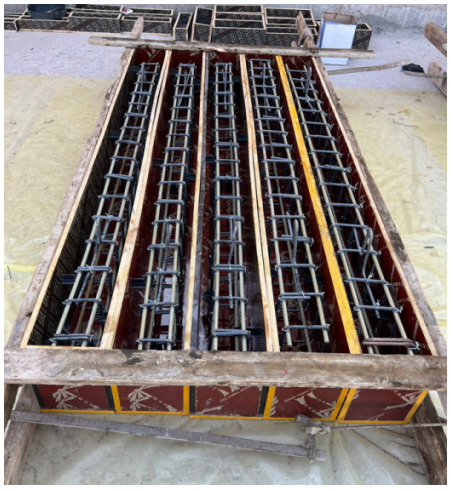

Fig. 4. Wooden molds and steel reinforcement cage of beams.

The furnace was constructed from a 5 mm thick steel plate in a box shape to accommodate the simultaneous combustion of multiple specimens. As illustrated in Figure 5, the internal dimensions were 60 cm height, 200 cm width, and 300 in length. The present study utilized 12 methane flame nozzles and 4 compressed air nozzles, all situated at the lower level of the furnace. Numerous tiny apertures for ventilation and thermocouple wires were situated at the top layer of the furnace. Figure 6 shows the thermometer and thermocouple.

Six beams were exposed to 500 °C and another six beams were exposed to 700 °C, as listed in Table I. Subsequently, all charred beams were let to cool by being left at ambient laboratory temperature. The temperature was measured using a digital thermometer equipped with a kind of K thermocouple sensor, fixed at the upper gap between the beam and the furnace cover according to the standard fire test standards, as can be seen in Figure 7 and in [16].

Fig. 5. The furnace.

a- 500°C target temperature b- 700°C target temperature

Fig. 6. Thermometer and thermocouple.

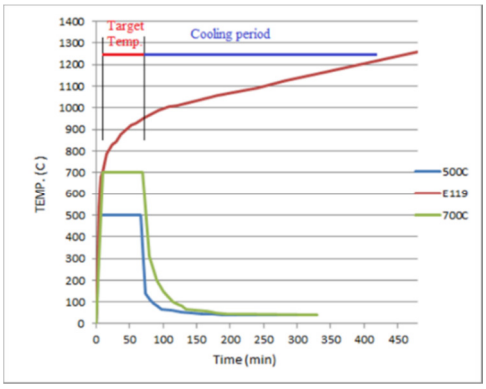

Fig. 7. Fire scenarios used in the burning test.

The testing apparatus was established at the Structural Laboratory of the Department of Civil Engineering, College of Engineering, University of Diyala, as shown in Figure 8.

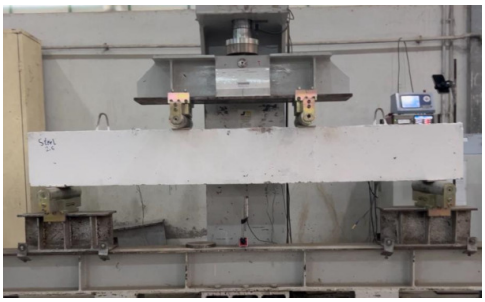

Fig. 8. Beam test setup.

III. MONOTONIC LOAD TEST POST-FIRE RESULTS AND DISCUSSION

A comparative analysis was conducted on the test findings and behavior of the burned beams about/and the control beams.

A. Load-Deflection Relationship for/of Beams

Figures 9-12 demonstrate that all examined beams with GFRP bars deflected linearly as the applied force progressed to some amount of ultimate load. After the cracking load reached a load of 25 kN to 40 kN, the examined beams exhibited linear deflection with increasing load. However, the slope of the deflection lines was significantly reduced compared to the pre-cracking phase. The deflection curves diverged according to the extent of cracking and the rate of stiffness degradation. The inclination of this linear section varied amongst specimens from the same group. The magnitude of the variation of curves is determined mostly by the main bar type, concrete cover thickness, type of protection, and exposure temperature. Cracks began to emerge in numerous places along the tested beams during the nonlinear stage, and subsequently grew and spread, as did the post-fire cracks. Figure 9 shows that the plastering of 1 cm was better than the fire-resistant dye as a form of protection against burning. Figure 10 exhibits that the stiffness of all beams diminished with rising burning temperatures. This is due to the degradation of concrete when exposed to fire, which results in increased beam deflection. Figure 11 illustrates the effect of different bar types.

(a)

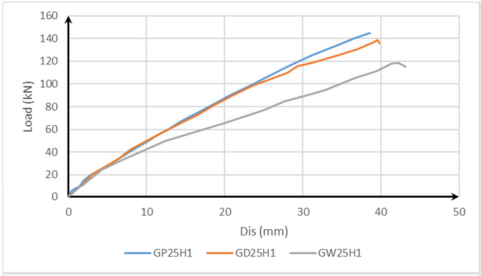

(b)

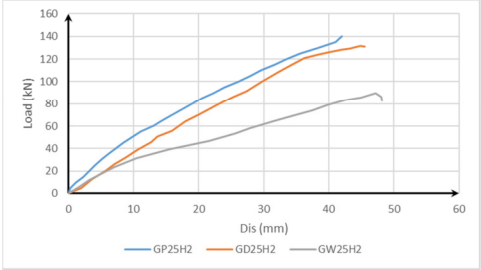

(c)

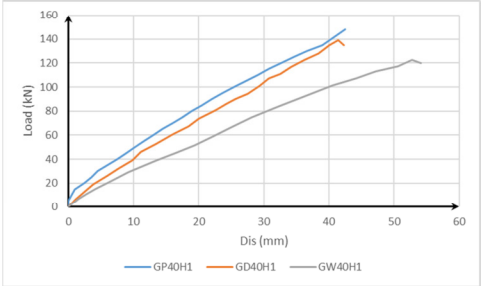

(d)

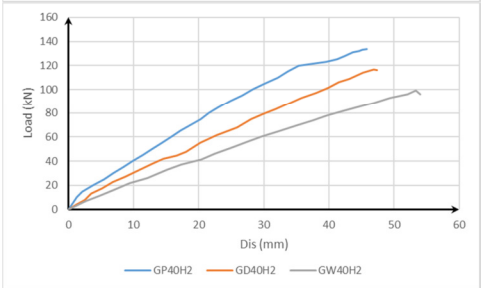

Fig. 9. Continued effect of protection type on load-deflection curves. (blue= plastering, red= Fire-resistant dye, gray= without protection). (a) Beams with cover=25 mm and temp.=500°C, (b) Beams with cover=25 mm and temp.=700 °C, (c) Beams with cover=40 mm and temp.=500 °C, (d) Beams with cover=40 mm and temp =700 °C.

(a)

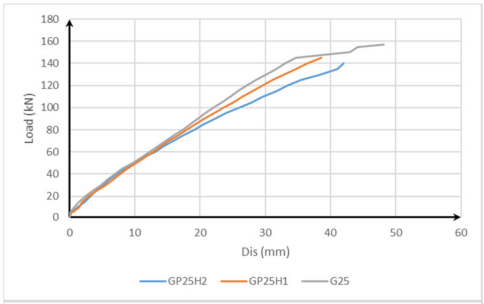

(b)

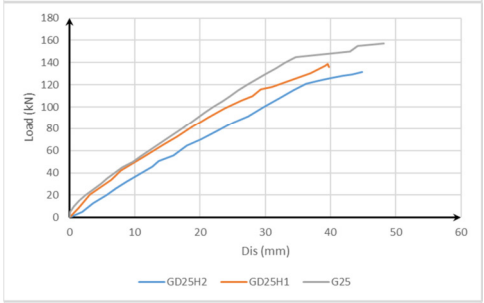

(c)

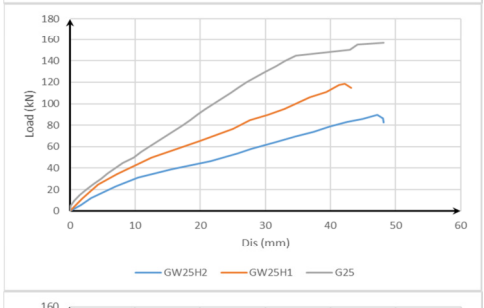

(d)

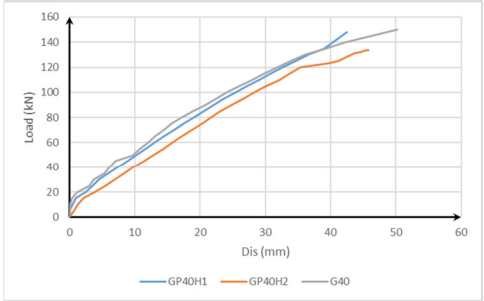

(e)

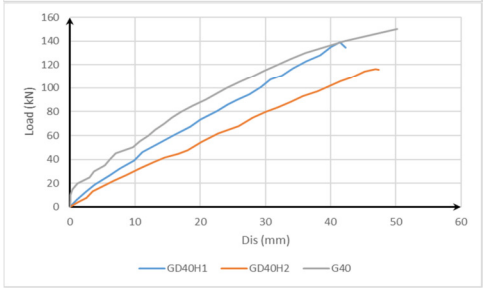

(f)

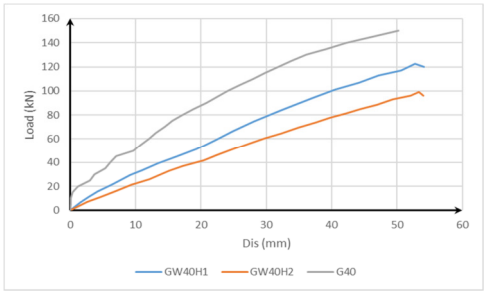

Fig. 10. Continued effect of burning temperature on load-deflection curves (H1= 500°C, H2= 700°C). (a) Beams with cover=25 mm and plastering. (b) Beams with cover=25 mm and Fire-resistant dye. (c) Beams with cover=25 mm without protection. (d) Beams with cover=40 mm and plastering. (e) Beams with cover=40 mm and Fire-resistant dye. (f) Beams with cover=40 mm without protection.

(a)

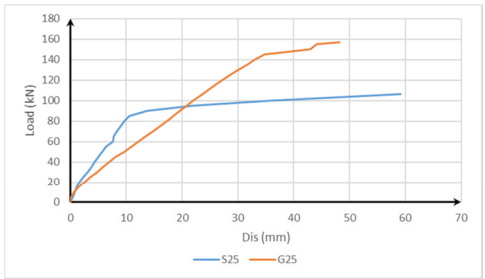

(b)

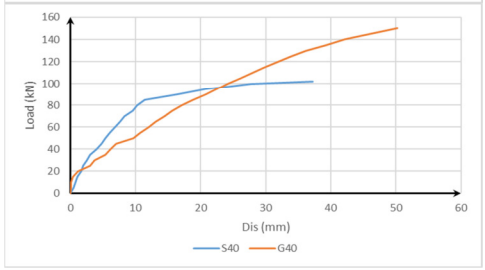

Fig. 11. Effect of bar type (s=steel and G= GFRP) on load-deflection curves. (a) Unburned Beams with concrete cover=25 mm. (b) Unburned Beams with concrete cover=40 mm.

TABLE V. EFFECT OF PROTECTION TYPE ON THE ULTIMATE LOAD

Group	Beam ID	Failure load P_{ult}, (kN)	Percentage of reduction in P_{ult} (%)
Cover 25 mm	G25	157	Ref.
	GP25H1	145	7.64
	GD25H1	139	11.46
	GW25H1	118.7	24.39
	GP25H2	140	10.82
	GD25H2	131.6	16.17
	GW25H2	89.7	42.86
Cover 40 mm	G40	150	Ref.
	GP40H1	148	1.33
	GD40H1	139.1	7.26
	GW40H1	122.4	18.4
	GP40H2	133.5	11
	GD40H2	116.5	22.33
	GW40H2	99.2	33.86

B. Load-Carrying Capacity and Failure Mode

Table V portrays the effect of the protection type on the ultimate load. Table VI depicts the effect of the burning temperature on the ultimate load, while Table VII shows the effect of the bar type on the ultimate load.

TABLE VI. EFFECT OF BURNING TEMPERATURE ON ULTIMATE LOAD

Group	Beam ID	Failure load P_{ult}, (kN)	Percentage of reduction in P_{ult} (%)
Cover 25 mm	G25	157	Ref.
	GP25H1	145	7.64
	GP25H2	140	10.8
	G25	157	Ref.
	GD25H1	139	11.5
	GD25H2	131.6	16.18
	G25	157	Ref.
	GW25H1	118.7	24.4
	GW25H2	89.7	42.9
Cover 40 mm	G40	150	Ref.
	GP40H1	148	1.33
	GP40H2	116.5	22.33
	G40	150	Ref.
	GD40H1	139.1	7.27
	GD40H2	116.5	22.337
	G40	150	Ref.
	GW40H1	122.4	18.4
	GW40H2	99.2	33.87

TABLE VII. EFFECT OF BAR TYPE ON THE ULTIMATE LOAD

Group	Beam ID	Failure load P ult (kN)	Percentage of reduction in P_{ult} (%)
Cover 25 mm	G25	157	Ref.
	S25	106.2	32.4
Cover 40 mm	G40	150	Ref.
	S40	102	32
G = GFRP bars, and S = Steel bars			

All beam failures originated from fractures at the beam soffit during the maximum bending moment. These fractures progressed upward due to steel yielding, ultimately leading to compression failure at the load points, characteristic of flexural failure. Figures 12-27 illustrate the failure modes of the tested beams.

Fig. 12. Cracks at the failure of the S25 beam.

Fig. 13. Cracks at the failure of the G25 beam.

Fig. 14. Cracks at the failure of the GP25H1 beam.

Fig. 15. Cracks at the failure of the GD25H1 beam.

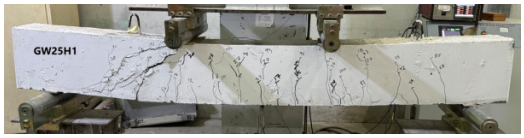

Fig. 16. Cracks at the failure of the GW25H1 beam.

Fig. 17. Cracks at the failure of the GP25H2 beam.

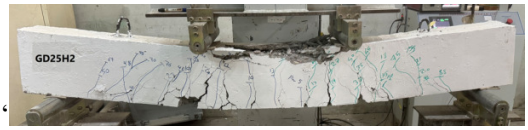

Fig. 18. Cracks at the failure of the GD25H2 beam.

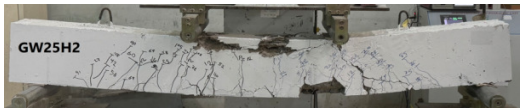

Fig. 19. Cracks at the failure of the GW25H2 beam.

Fig. 20. Cracks at the failure of the S40 beam.

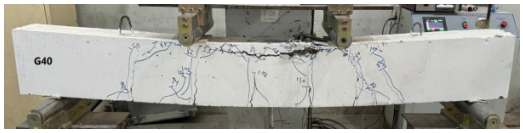

Fig. 21. Cracks at the failure of the G40 beam.

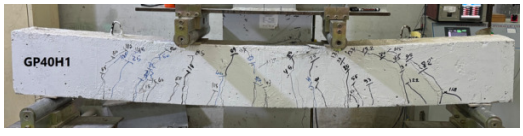

Fig. 22. Cracks at the failure of the GP40H1 beam.

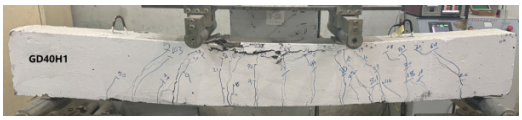

Fig. 23. Cracks at the failure of the GD40H1 beam.

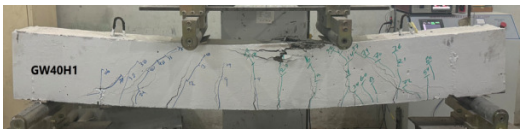

Fig. 24. Cracks at the failure of the GW40H1 beam.

Fig. 25. Cracks at the failure of the GP40H2 beam.

Fig. 26. Cracks at the failure of the GD40H2 beam.

Fig. 27. Cracks at the failure of the GW40H2 beam.

IV. CONCLUSION

The research variables consist of the type of the main bar material, protection type against fire, concrete cover thickness, and the burning temperature. Most of the ongoing research focuses on the short-term performance and immediate effects of heat. There is a lack of extensive data regarding how GFRP beams respond to different temperature regimes comparable to realistic fire settings under the effect of many types of fire protection and different concrete cover thicknesses. Thus, there is a need for reliable data that can predict the structural performance of such beams under fire in terms of experimental data. From the results presented in this research, it can be concluded that:

- Load-deflection curves show that the stiffness of all beams diminishes at elevated burning temperatures due to the degradation of concrete during fire exposure, leading to an increase in beam deflection under the same load.
- Concerning the group with a 25 mm cover, the ultimate load of the beam with plastering protection decreased by 7.64% and 10.82% for/at the burning temperatures of 500°C and 700°C, respectively, compared to the reference unburned beam. The ultimate load of the beam with fire-resistant dye decreased by 11.46% and 16.17% for/at the burning temperatures of 500°C and 700°C, respectively, compared to the control unburned beam. The same behavior was observed in the group with a 40 mm cover. So, the plastering of 1 cm was better than the fire-resistant dye as a form of protection against burning.
- Concerning the group with a 25 mm cover and plastering, the ultimate load of the beam decreased by 7.64% and 10.8% for/at the burning temperatures of 500°C and 700°C, respectively, compared to the similar unburned beam. The ultimate load of the beam without any protection decreased by 24.4% and 42.9% for/at the burning temperatures of 500°C and 700°C, respectively, compared to the similar unburned beam. The same behavior was observed in the group with a 40mm cover. The maximum load capacity of all tested beams diminished with rising combustion temperature due to the degradation of concrete when subjected to fire.
- The ultimate load of the GFRP bars beam had a higher value than the steel bars beam. For the group with a 25 mm cover, the ultimate load of the beam with steel bars was reduced by 32.4% compared to a similar beam with GFRP bars. For the group with a 40 mm cover, the ultimate load of the beam with steel bars decreased by 32% compared to the similar beam with GFRP bars.
- All beam failures originated from fractures at the beam soffit, where the bending moment was at its maximum. These fissures propagated toward the upper zone due to steel yielding, culminating in compression failure at the load points, indicative of flexural failure.

REFERENCES

[1] H. A. Al-Baghdadi and A. Sabah, "Behavior of RC Beams Strengthened with NSM-CFRP Strips Subjected to Fire Exposure: A Numerical Study," *Engineering, Technology & Applied Science Research*, vol. 11, no. 6, pp. 7782–7787, Dec. 2021, https://doi.org/10.48084/etasr.4493.

[2] B. Abdulkareem and A. F. Izzet, "Serviceability of Post-fire RC Rafters with Openings of Different Sizes and Shapes," *Journal of Engineering*, vol. 28, no. 1, pp. 19–32, Jan. 2022, https://doi.org/10.31026/j.eng.2022.01.02.

[3] B. F. Abdulkareem, A. F. Izzet, and N. Oukaili, "Post-Fire Behavior of Non-Prismatic Beams with Multiple Rectangular Openings Monotonically Loaded," *Engineering, Technology & Applied Science Research*, vol. 11, no. 6, pp. 7763–7769, Dec. 2021, https://doi.org/10.48084/etasr.4488.

[4] A. Kareem and S. D. Mohammed, "The Experimental and Theoretical Effect of Fire on the Structural Behavior of Laced Reinforced Concrete Deep Beams," *Engineering, Technology & Applied Science Research*, vol. 13, no. 5, pp. 11795–11800, Oct. 2023, https://doi.org/10.48084/etasr.6272.

[5] Z. K. Al-Mamory and A. H. A. Al-Ahmed, "Behavior of steel fiber reinforced concrete beams with CFRP wrapped lap splice bars," *Structures*, vol. 44, pp. 1995–2011, Oct. 2022, https://doi.org/10.1016/j.istruc.2022.08.096.

[6] M. Abdulkhaliq and A. H. Al-Ahmed, "Behavior of GFRP Reinforced-Concrete Bubbled One-Way Slabs by Encased Composite Steel I-Sections," *Engineering, Technology & Applied Science Research*, vol. 14, no. 5, pp. 16701–16712, Oct. 2024, https://doi.org/10.48084/etasr.8123.

[7] B. F. Abdulkareem and A. F. Izzet, "Post Fire Residual Concrete and Steel Reinforcement Properties," *IOP Conference Series: Earth and Environmental Science*, vol. 856, no. 1, Jun. 2021, Art. no. 012058, https://doi.org/10.1088/1755-1315/856/1/012058.

[8] A. Sadek, M. El-Hawary, and A. El-Deeb, "Fire Resistance Testing of Concrete Beams Reinforced by GFRP Rebars," *Journal of applied fire science*, vol. 14, no. 2, pp. 91–104, 2005.

[9] K. H. Tan and Y. Zhou, "Performance of FRP-Strengthened Beams Subjected to Elevated Temperatures," *Journal of Composites for Construction*, vol. 15, no. 3, pp. 304–311, Jun. 2011, https://doi.org/10.1061/(ASCE)CC.1943-5614.0000154.

[10] B. Yu and V. K. R. Kodur, "Factors governing the fire response of concrete beams reinforced with FRP rebars," *Composite Structures*, vol. 100, pp. 257–269, Jun. 2013, https://doi.org/10.1016/j.compstruct. 2012.12.028.

[11] J. Zhao, G. Li, Z. Wang, and X.-L. Zhao, "Fatigue behavior of concrete beams reinforced with glass- and carbon-fiber reinforced polymer (GFRP/CFRP) bars after exposure to elevated temperatures," *Composite Structures*, vol. 229, Dec. 2019, Art. no. 111427, https://doi.org/ 10.1016/j.compstruct.2019.111427.

[12] H. Al-Thairy and N. H. Al-hasnawi, "Behavior and Failure Mode of GFRP bars RC Beams under Elevated Temperature," *IOP Conference Series: Materials Science and Engineering*, vol. 888, no. 1, 2020, Art. no. 012012, https://doi.org/10.1088/1757-899X/888/1/012012.

[13] N. H. Albu-Hassan and H. Al-Thairy, "Experimental and numerical investigation on the behavior of hybrid concrete beams reinforced with GFRP bars after exposure to elevated temperature," *Structures*, vol. 28, pp. 537–551, Dec. 2020, https://doi.org/10.1016/j.istruc.2020.08.079.

[14] J. Prokeš, I. Rozsypalová, F. Girgle, P. Daněk, and P. Štěpánek, "Effects of elevated temperature on the behaviour of concrete beams reinforced with fiber reinforced polymers," *IOP Conference Series: Materials Science and Engineering*, vol. 1039, no. 1, Jan. 2021, Art. no. 012008, https://doi.org/10.1088/1757-899X/1039/1/012008.

[15] A. N. Abdullah and M. M. Kassim, "Residual Strength of Concrete Beams Reinforced with GFRP Bars Exposed to Elevated Temperatures," *Tikrit Journal of Engineering Sciences*, vol. 31, no. 3, pp. 18–31, Sep. 2024, https://doi.org/10.25130/tjes.31.3.3.

[16] *Standard Test Methods for Fire Tests of Building Construction and Materials*. USA: ASTM International, 2016.